

Structural and insulator-metal quantum phase transitions on a lattice

E. V. Tsiper and A. L. Efros

Department of Physics, University of Utah, Salt Lake City, Utah 84112

(Received 26 August 1997)

We consider a two-dimensional gas of spinless fermions with Coulomb and short-range interactions on a square lattice at $T=0$. Using the exact-diagonalization technique we study finite clusters up to 16 particles at filling factors $\nu=1/2$ and $1/6$. By increasing the hopping amplitude we obtain the low-energy spectrum of the system in a wide range from the classical Wigner crystal to an almost free gas of fermions. Particular effort is made to study the mechanism of the structural and insulator-metal transitions. We show that both transitions are determined by the energy band of the defect with the lowest energy in the Wigner crystal. [S0163-1829(98)08008-4]

I. INTRODUCTION

The insulator-metal (IM) transition and the role of electron-electron interaction in this transition is a problem of permanent interest, both theoretical and experimental. It has been shown¹⁻³ that in the systems with strong disorder the interaction is in favor of delocalization because electrons may help each other to overcome the random potential. In clean systems the role of the interaction is opposite. It may create the so-called correlated insulator in a system that would be metallic otherwise. The Wigner crystal (WC) is a good example of such an insulator.

The WC in continuum is not an insulator itself, since it can move as a whole and carry current. However, due to shear modulus it can be pinned by a small disorder. The ground-state energy of the continuum WC and its zero-temperature melting were widely studied in recent years both with and without magnetic field.⁴

In contrast to the continuum case, the WC on a lattice can be an insulator without any disorder due to the Umklapp processes in a host lattice. The WC on a lattice does not have any sound or soft plasma modes and its excitation spectrum has a gap.

The great majority of the efforts made recently to study correlated particles on a lattice were restricted to the Hubbard model or the t - J model (see review Ref. 5). The so-called extended Hubbard model with short-range and long-range interactions has been mostly considered for bosons in connection to the insulator-superconductor transition.⁶⁻⁹ In these papers supersolid and superfluid phases have been found. The bosons with infinite on-site repulsion are called hard-core bosons. In the case of the nearest-neighbor interaction the hard-core boson problem maps into an Ising-Heisenberg spin Hamiltonian.

Spinless fermions are similar to the hard-core bosons. In both systems the number of particles on a site is either zero or one. In the one-dimensional (1D) case these two systems are equivalent if the interaction between particles does not permit them to penetrate through one another.¹⁰

The 1D problem with the nearest-neighbor interaction at half filling is exactly soluble.¹¹⁻¹³ This instructive solution shows that the transition is not of the first order and that the IM transition, as detected by the stiffness constant, appears at

the same point as the structural transition.¹³

Very few works exist on the extended Hubbard model for 2D fermions. Pikus and Efros¹⁴ have performed a computer modeling for 2D spinless fermions with Coulomb interaction on a square lattice at filling factors $\nu=1/3$ and $1/6$. They argue that the lifting of the ground-state degeneracy with increasing J is a very good diagnostic of the structural phase transition. They have also found a similarity between the systems of spinless fermions and hard-core bosons near the transition.

In this paper we study structural and IM transitions for spinless fermions at $\nu=1/2$ and $1/6$. To detect these transitions we use the ground-state splitting and the flux sensitivity,^{15,16} respectively. The purpose of the work is to take advantage of the exact diagonalization technique and to study the modification of the low-energy part of the spectrum in a wide interval of the hopping amplitude J all the way from the classical WC to the free fermion limit.

Our results for long-range and short-range interactions suggest a simple picture of the transition. The transition is related mainly to the modification of the two lowest branches of the energy spectrum. At small J these two branches are the WC state and the energy band of the defect with the lowest energy.

The paper is organized as follows. In Sec. II we describe our numerical technique and present some general results. Section III contains the results of computations and their discussion. We suggest the mechanism of the transition, analyze the role of the size effect in finite-cluster computations, and discuss the possibility that the delocalized phase above the IM transition is superconducting. To better illustrate the mechanism of the transition we present the dependence of the total energy on the quasimomentum, $E(P)$, for a 1D system with $1/r$ interaction.

II. COMPUTATIONAL APPROACH AND GENERAL REMARKS

We consider spinless fermions at $T=0$ on the 2D square lattice described by the following model Hamiltonian:

$$H = J \sum_{\mathbf{r}, \mathbf{s}} a_{\mathbf{r}+\mathbf{s}}^\dagger a_{\mathbf{r}} \exp(i\phi_{\mathbf{s}}) + \frac{1}{2} \sum_{\mathbf{r} \neq \mathbf{r}'} n_{\mathbf{r}} n_{\mathbf{r}'} V(|\mathbf{r} - \mathbf{r}'|). \quad (1)$$

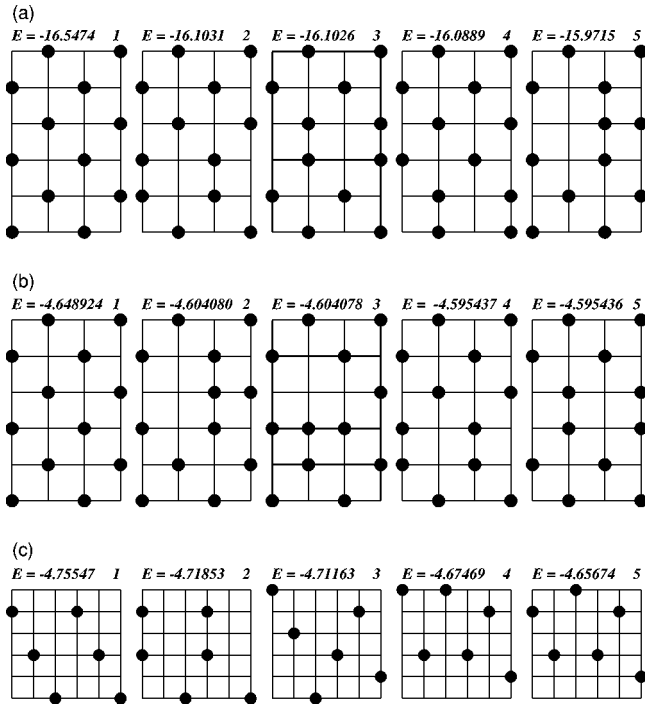


FIG. 1. Five icons with the lowest energies for (a) $\nu=1/2$, LR interaction, (b) $\nu=1/2$, SR interaction, and (c) $\nu=1/6$ LR interaction.

Here $n_{\mathbf{r}} = a_{\mathbf{r}}^{\dagger} a_{\mathbf{r}}$, the summation is performed over the lattice sites \mathbf{r}, \mathbf{r}' and over the vectors of translations \mathbf{s} to the nearest-neighbor sites. We consider long-range (LR) Coulomb potential $V(r) = 1/r$ and short-range (SR) strongly screened Coulomb potential $V(r) = \exp(-r/r_s)/r$ with $r_s = 0.25$ in the units of lattice constant. We study rectangular clusters $L_x \times L_y$ with the periodic boundary conditions. The dimensionless vector potential $\boldsymbol{\phi} = (\phi_x, \phi_y)$ in the Hamiltonian is equivalent to the twist of the boundary conditions by the flux $\Phi_i = L_i \phi_i$, $i = x, y$. The energy spectrum is periodic in Φ_x and Φ_y with the period 2π .

As a basis for computations we use many-electron wave functions at $J=0$ in the coordinate representation: $\Psi_{\alpha} = \prod_{i=1}^N a_{\mathbf{r}_i}^{\dagger} |\text{VAC}\rangle$. The total size of the Hilbert space is C_M^N , where $M = L_x \times L_y$ is the area of a system, and N is the number of particles.

The basic functions Ψ_{α} can be visualized as pictures, which we call *icons*. Some lowest-energy icons are shown in Fig. 1. The energy of each icon is calculated as a Madlung sum, assuming that the icon is repeated periodically over the infinite plane with a compensating homogeneous background.

The icon with the lowest energy is a fragment of the crystal. The icons with higher energies represent different types of defects in the WC.

A. Quasimomentum representation

The Hamiltonian Eq. (1) is translationally invariant. For each icon α there are m_{α} different icons that can be obtained from it by various translations. These icons are combined to get the wave function with total quasimomentum \mathbf{P} :

$$\Psi_{\alpha\mathbf{P}} = \frac{1}{\sqrt{m_{\alpha}}} \sum_{\mathbf{r}} \exp(i\mathbf{P}\mathbf{r}) T_{\mathbf{r}} \Psi_{\alpha}. \quad (2)$$

The summation is performed over m_{α} translations $T_{\mathbf{r}}$. This transformation reduces the effective Hilbert space size by approximately M times.

For the icons with periodic structures the number m_{α} of different functions $\Psi_{\alpha\mathbf{P}}$ is smaller than M . For example, the icon Ψ_0 of the WC with one electron per primitive cell generates $m_0 = 1/\nu$ different values of \mathbf{P} . These values are determined by the conditions

$$(-1)^{Q_j} \exp(i\mathbf{P}l_j) = 1. \quad (3)$$

Here l_j are the primitive vectors of the WC, and Q_j are the numbers of fermionic permutations necessary for translations on these vectors. These conditions can be easily understood. If translation on a vector l_j is applied to Eq. (2), the right-hand side acquires a factor $(-1)^{Q_j}$, while for a function with given \mathbf{P} this factor must be equal to $\exp(i\mathbf{P}l_j)$. If Q_j are even for both l_j , the allowed \mathbf{P} form the reciprocal lattice of the WC. However, in the case when one or both of Q_j are odd, the lattice is shifted by π in the corresponding directions. In such case $\mathbf{P}=0$ is forbidden. The complete set of m_{α} nontrivial values of \mathbf{P} can be obtained by restricting \mathbf{P} to the first Brillouin zone of the background lattice. One WC is represented by a number of icons obtained from each other by the point-group transformations of the background lattice.

Note that the total number of allowed values of \mathbf{P} for the WC is the property of the WC and it remains finite at infinite cluster size. On the contrary, an icon representing a point defect in a WC generates all vectors \mathbf{P} . Their total number is equal to the volume M of the first Brillouin zone of the background lattice.

B. General remarks

In the macroscopic system all the states generated by the WC icon form the ground state degenerate at small J . This degeneracy appears because the effective matrix elements that connect translated WC's are zero in the macroscopic limit. The total energy as a function of quasimomentum \mathbf{P} has identical minima at all \mathbf{P} generated by the WC icons. The spectra of excitations in the vicinity of these minima are also identical.

The charge density for the state with given quasimomentum \mathbf{P} [see Eq. (2)] is always the same at all sites of the host lattice. However, at small J the correlation function indicates a long-range order. Any small perturbation, that violates translational invariance splits the degeneracy in such a way that the ground state describes a single WC with a strong modulation of the charge density.

The lifting of the ground-state degeneracy at some critical value J_c indicates a structural phase transition and restoration of the host lattice symmetry.

The flux sensitivity of a macroscopic system is zero at small J . It becomes nonzero at some finite value of J that might be different from J_c . We associate this transition with the IM transition.¹⁵

For the finite system the following results can be obtained directly using the perturbation theory with respect to J :

(i) The ground state and the lowest excited states have a large common negative shift that is proportional to J^2 and to the total number of particles N . This shift is the same for all low-lying states and does not affect the excitation spectrum of the system.

(ii) At $\nu=1/2$ the splitting of the ground state appears in the N th order and is proportional to J^N . At other filling factors the degeneracy of the ground state at $J=0$ is larger than two. The splitting is determined by matrix elements, which are proportional to J^K . For each matrix element the value of K is equal to the number of hops necessary to obtain one crystalline structure from another and is proportional to N .

(iii) The flux dependence of the ground state for the flux in the x direction appears in the L_x th order and is proportional to J^{L_x} in the 2D case. In 1D the flux dependence appears in the N th order and is proportional to J^N .

Thus, we conclude that both the lifting of the ground-state degeneracy and the appearance of the flux sensitivity occur very sharply and they can be used as convenient criteria for the structural and the IM transitions, respectively. Note that the correlation function is a less sensitive criterion for small clusters^{14,18} since it does not exhibit sharp behavior in the transition region.

III. RESULTS OF COMPUTATIONS AND DISCUSSION

A. Results of computations

Figures 2(a) and 2(b) show the results of diagonalization for cluster 4×6 with 12 electrons for the LR (a) and SR (b) interactions. The total energy E is shown as a function of J . The ground-state energy is taken as a reference point for E . Here and below, the unit of energy is the LR interaction energy between nearest neighbors. At $J=0$ the values of E coincide with the energies of the icons shown in Fig. 1. We define Δ as the gap between the ground and first excited states at $J=0$. Note that Δ in the LR case is almost exactly 10 times larger than in the SR case [see Figs. 1(a) and 1(b)].

At large J the energy E is linear in J . Thus, we can conclude that with increasing J in this interval we go all the way from classical icons to free fermions. The ground state is almost degenerate at small J and it splits into two states with increasing J . As we have discussed above, this is a manifestation of the structural transition. The quasimomenta of these two states, $\mathbf{P}=(0,\pi)$ and $(\pi,0)$, are those generated by the WC icon. In Figs. 2(a) and 2(b) they are denoted as $(0,3)$ and $(2,0)$, where (n_x, n_y) stands for quasimomentum with projections $P_x=2\pi n_x/L_x$, $P_y=2\pi n_y/L_y$. The other branches are the bands of defects.

Figures 3(a) and 3(b) show flux sensitivity $\delta E=|E(\pi)-E(0)|$, computed for the ground state for two directions of the vector potential. Here $E(\Phi)$ stands for the total energy as a function of Φ_x or Φ_y . In accordance with perturbation theory (see Sec. II B), the flux sensitivity at small J obeys the laws J^4 and J^6 for the direction of the vector potential along the short and long sides of the cluster, respectively. The energy splitting between the lowest states with $\mathbf{P}=(0,\pi)$ and $(\pi,0)$ is also shown. At small J the splitting is proportional to J^{12} (12 is the number of particles), as it follows from the perturbation theory.

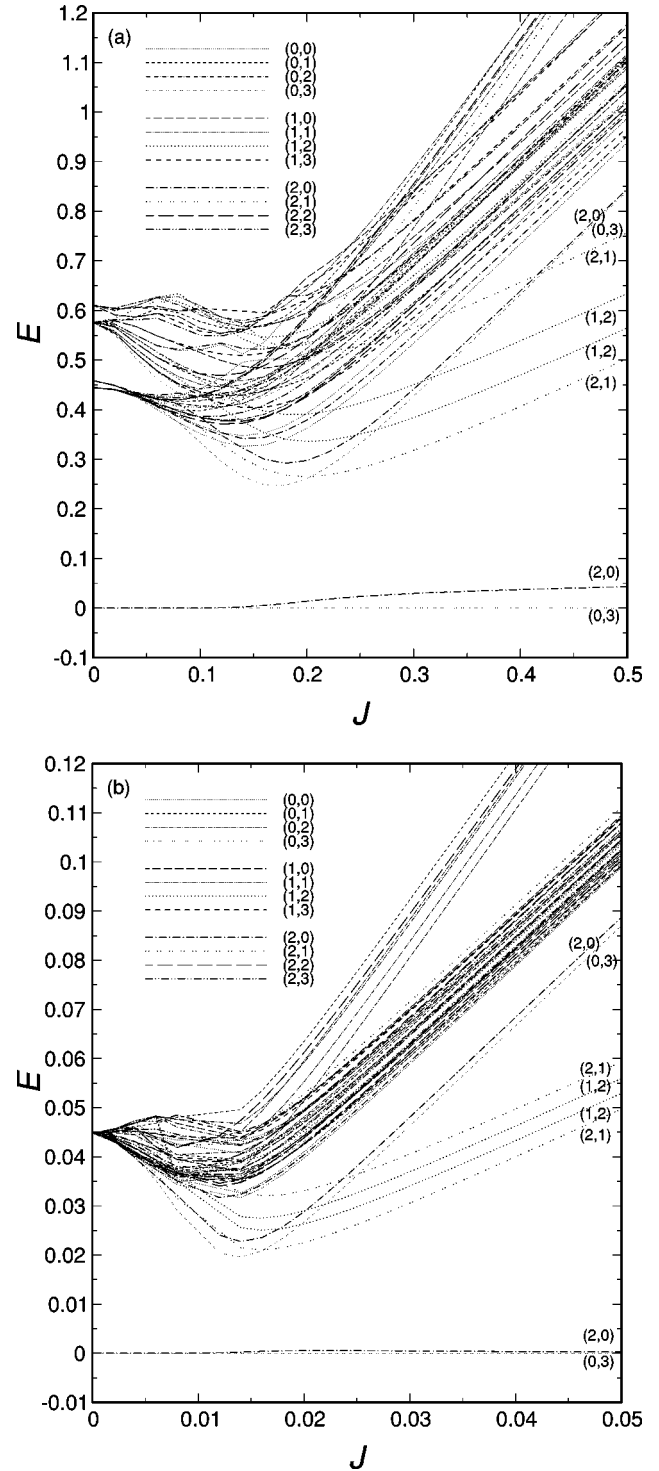


FIG. 2. Low-energy part of the spectrum as a function of J for the 4×6 cluster at $\nu=1/2$ for LR (a) and SR (b) interactions. The numbers (n_x, n_y) denote the components of quasimomentum $\mathbf{P}=(2\pi n_x/L_x, 2\pi n_y/L_y)$. The ground-state energy is taken as a reference point.

At large J the flux sensitivity is linear in J and coincides with the free-fermion value. Note that for free fermions at $\nu=1/2$ the flux sensitivity δE is size independent for large clusters.¹⁷

The intervals δJ where computational curves for δE make a crossover from one asymptotic to another are pretty narrow. In what follows we assume that these are the critical

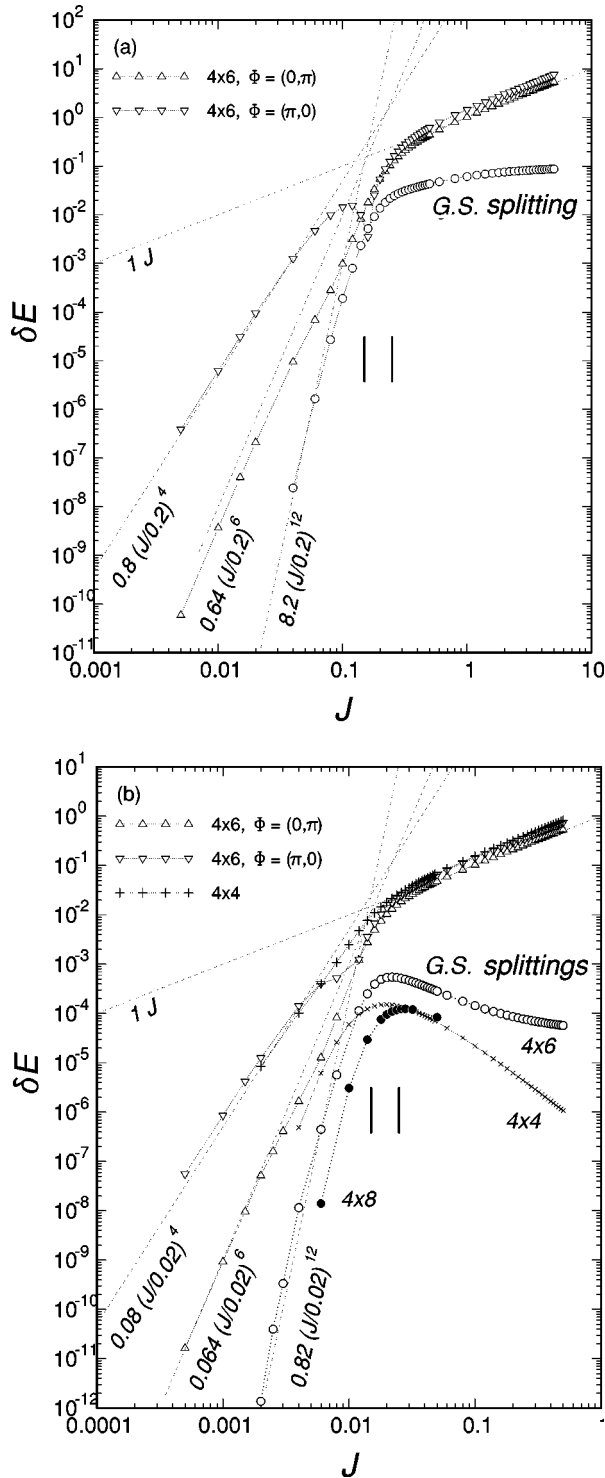


FIG. 3. Flux sensitivity for two directions of vector potential and the ground-state splitting as a function of J at $\nu=1/2$. (a) LR interaction for a cluster 4×6 . (b) SR interaction for 4×4 , 4×6 , and 4×8 clusters. Dashed lines show large- J and small- J asymptotic as obtained by the best fit with correct powers of J . The vertical bars show the critical region of the transition.

intervals for the IM transition, smeared in a finite cluster. These critical intervals can be fairly well defined for each cluster and should shrink into a transition point with increasing cluster size.

The vertical bars in Figs. 3(a) and 3(b) show the estimated critical interval δJ for the IM transition, which is approxi-

mately 0.15–0.25 for the LR interaction and 0.015–0.025 for the SR interaction in the 4×6 cluster.

The behavior of the ground-state splitting (GSS) at large J is more complicated. In the free-fermion approximation the GSS is zero. Considering interaction as perturbation one can show that in the 4×4 cluster the $GSS \rightarrow 0$ as $J \rightarrow \infty$. In the 4×6 cluster the $GSS \rightarrow 5.76 \times 10^{-5}$ for the SR interaction and the $GSS \rightarrow 0.14$ for the LR interaction as $J \rightarrow \infty$. These analytical calculations are in good agreement with the computational results at large J given in Figs. 3(a) and 3(b). In the case of SR interaction the GSS curve has a maximum. It is reasonable to assume that the crossover from the WC to free fermions occurs in the vicinity of this maximum. There is no maximum in the case of LR interaction and the crossover region can be estimated using the sharp maximum of the second derivative.

We conclude that within the accuracy of our computations, limited by the finite cluster sizes, the IM transition detected by the flux sensitivity and structural transition detected by the GSS occur simultaneously.

Comparison of Figs. 3(a) and 3(b) shows that the dependencies $\delta E(J)$ for the LR and SR potentials are almost indistinguishable if all the energy scales for one of them are adjusted 10 times. This factor is just the ratio of zero- J gaps Δ for these two cases. Thus, we come to the conclusion that J_c depends on the type of interaction potential mostly through the value of Δ . The same applies to the general structure of the low-energy spectrum of the system in the transition region as can be seen from comparison of Figs. 2(a) and 2(b).

Figures 4(a) and 4(b) show the data for $\nu=1/6$ and LR interaction. Figure 4(a) looks more complicated than Figs. 2(a) and 2(b). The WC for $\nu=1/6$ is shown in the first icon in Fig. 1(c). There are four such WCs which can be obtained from each other by point-symmetry operations. Each WC generates six different values of \mathbf{P} . Thus, at small J the ground state of the system is 24-fold degenerate. The degeneracy is high, however, it remains the same in the infinitely large cluster.

The primitive vectors of the WC at $\nu=1/6$ cannot be obtained from each other by any symmetry operation on the host lattice. This means that the WC phase belongs to a *reducible* representation of the symmetry group of the host lattice. Following Landau and Lifshitz,¹⁹ the symmetry reduction in the second-order phase transition should be such that the low-symmetry phase belongs to an irreducible representation of the symmetry group of the high-symmetry phase. We conclude that the single second-order phase transition is forbidden in this case. However, it can occur as a series of transitions, each reducing the symmetry one step further. In fact, Fig. 4(a) recalls the picture of multiple transitions. We think that each splitting of the energy levels generated by the WC icon manifests a structural transition. The 6×6 cluster is too small to distinguish the critical intervals for each of these transitions. We can only conclude from Figs. 4(a) and 4(b) that the critical interval δJ for all of the structural transitions and IM transition is 0.01–0.03. This interval is shown by vertical bars in Fig. 4(b).

B. The mechanism of transition

Our data suggest the following mechanism of the transition. The width of the band of the lowest defect in the WC

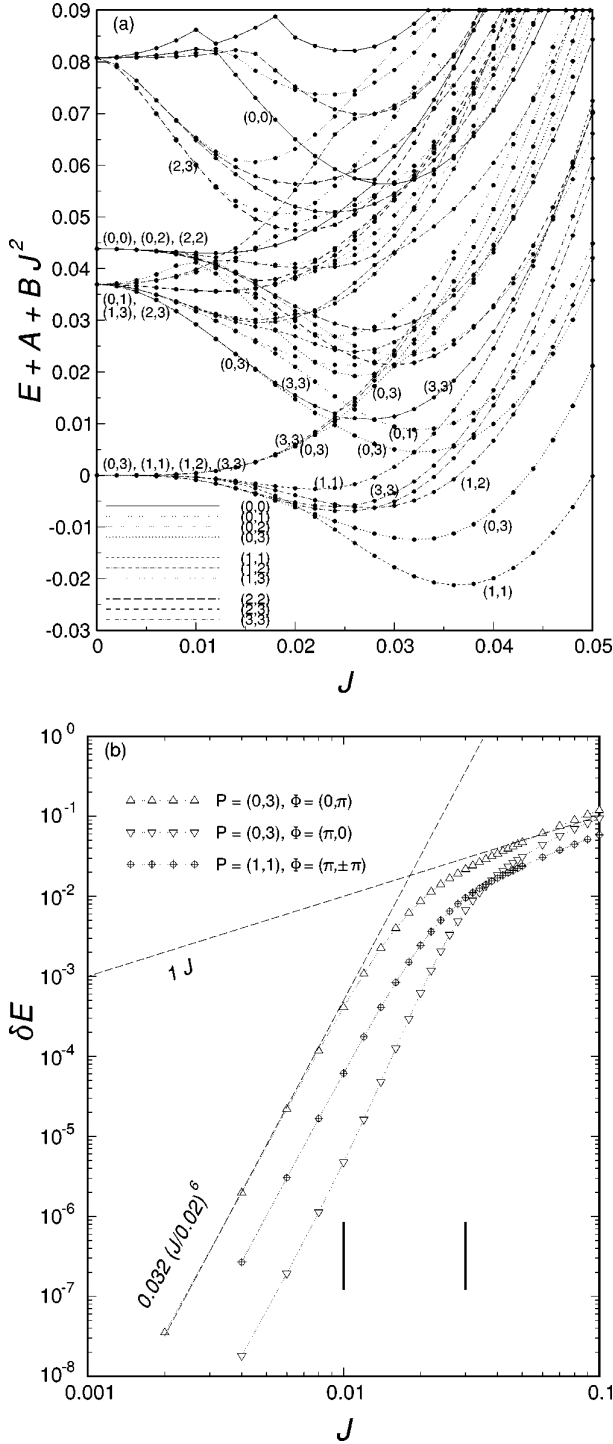


FIG. 4. Results for $\nu=1/6$, 6×6 cluster. (a) Low-energy part of the spectrum; (b) flux sensitivity for different P and two directions of vector potential. The numbers (n_x, n_y) denote the values of \mathbf{P} as in Fig. 2. The reference point is taken to be $A + BJ^2$, where A is the energy of the WC at $J=0$, and $B=177$ is the exact J^2 term as obtained from perturbation theory. Dashed lines have the same meaning as in Fig. 3. The vertical bars show the critical region of the transition.

increases with J such that its lowest edge comes close to the energy of the ground state¹⁸ [see Figs. 2(a) and 2(b), 4(a), and 5]. Strong mixing between the crystalline and defect states with the same quasimomentum occurs at this point. The avoided crossing appears between the ground state and the states in the defect band.

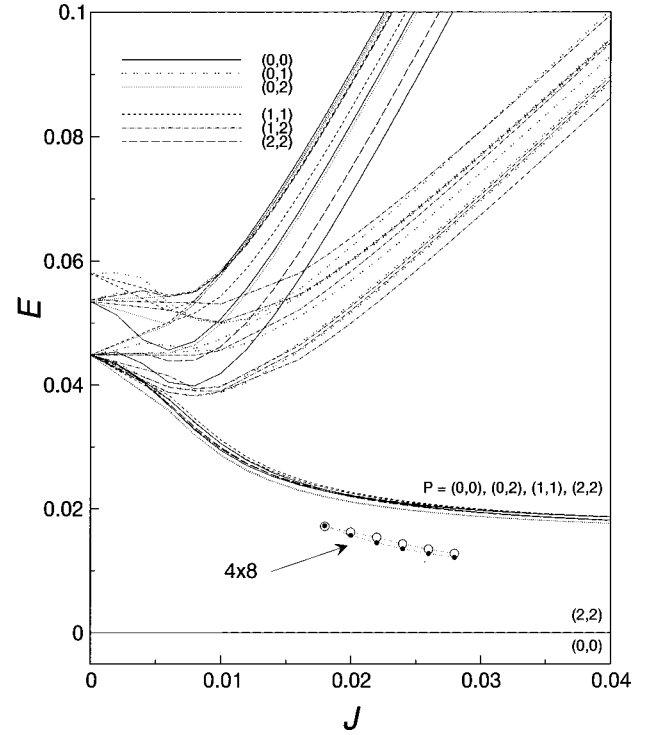


FIG. 5. The same as Fig. 2(b) for the 4×4 and 4×8 clusters. The data for the 4×8 cluster is presented for $\mathbf{P}=(0,0)$ (dots) and $\mathbf{P}=(\pi, \pi)$ (circles) only.

One can interpret the avoided crossing in terms of the ground state, which acquires a large admixture of defect states. This interpretation recalls the idea of zero-point defectons proposed by Andreev and Lifshitz.²⁰

In principle, one can imagine that the state with a quasimomentum \mathbf{P} different from those generated by the WC icon becomes the ground state via a branch crossing. However, in all cases we have considered, we observe the avoided crossing between the crystalline state and the state in the defect band with the same \mathbf{P} . Assuming that this is the case for larger clusters, we conclude that the phase transition is not of the first order.

The proposed mechanism of the transition can be illustrated by the dependence $E(\mathbf{P})$ at given J . Unfortunately, in the 2D case the number of discrete values of \mathbf{P} along any line in the first Brillouin zone is small even for the largest 2D system we study. To clarify our understanding of the transition it is instructive to analyze the data for 1D systems.

We have considered 1D systems with the nearest- and next-nearest-neighbor interaction²¹ and the system with LR interaction. In the latter case we study Hamiltonian Eq. (1) at filling factor $\nu=1/2$ and $V(i-j)=1/|i-j|$. In 1D we switch from the homogeneous background to the chain with $\pm 1/2$ charges for the empty and occupied sites respectively.

Figure 6 shows the results for the flux sensitivity vs J for different system sizes L . The sharp exponential behavior indicates that the system becomes an insulator at small J . This result clearly contradicts the statement by Poilblanc *et al.*²² that the 1D Coulomb system is metallic at all J . This result contradicts the prediction by Poilblanc *et al.*²² that the ground state of the 1D Coulomb system is metallic. Note,

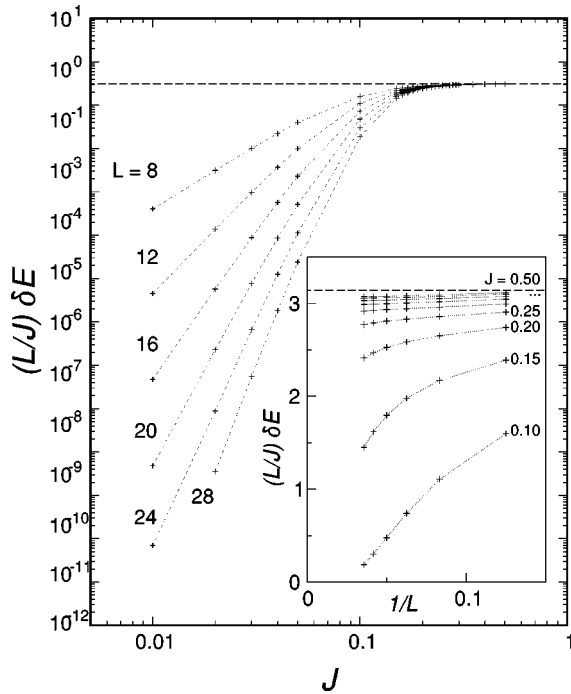


FIG. 6. Flux sensitivity in units J/L as a function of J for the 1D system with LR Coulomb interaction at $\nu=1/2$ for different sizes L . Long-dashed line shows the theoretical value $L\delta E/J=\pi$ for free fermions. The inset shows the extrapolation to $1/L\rightarrow 0$.

however, that this prediction is mostly based on computations for $\nu=1/3$, while we consider $\nu=1/2$.

An extrapolation to $1/L\rightarrow\infty$ shown in the inset gives a rather wide interval for J_c of the IM transition between 0.17 and 0.3.

Figure 7 shows a few lowest eigenvalues for each quan-

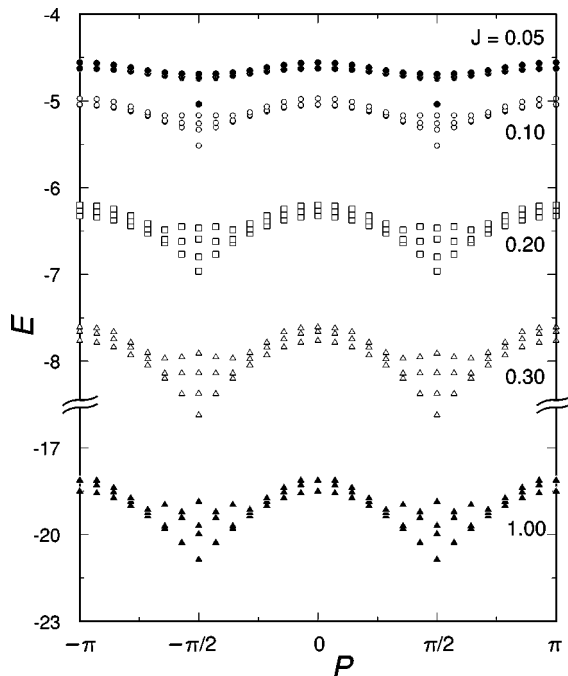


FIG. 7. The dependence of the total energy on the total quasi-momentum at different J for 1D system with LR Coulomb interaction at $\nu=1/2$ and size $L=28$.

TABLE I. Zero- J gaps Δ and estimated critical regions δJ for different systems studied.

System	δJ	J_m	Δ	J_m/Δ
$\nu=1/2$, LR, 4×6	0.15–0.25	0.2	0.444	0.45
$\nu=1/2$, SR, 4×6	0.015–0.025	0.02	0.0448	0.44
$\nu=1/6$, LR, 6×6	0.01–0.03	0.02	0.037	0.54

tized value of P for a cluster of 28 sites with 14 particles. Note that the spectrum has nontrivial symmetry around the points $P=\pm\pi/2$. This symmetry appears for even N at $\nu=1/2$ as a result of the particle-hole symmetry.

For even N the WC icon generates two states with quasi-momenta $P=\pm\pi/2$, which are degenerate at all J . As one can see from Fig. 7, at $J=0.05$ these states are separated by a gap from the continuum of states, generated by the icon of the point defect. At $J=0.1$ the defect band broadens and, as a result, the gap decreases. However, the lowest eigenvalue at $P=\pm\pi/2$ is still separated from the defect band, whereas the second eigenvalue belongs to it. At this point an avoided crossing starts to develop and the width of the gap remains almost unchanged from $J=0.1$ to $J=0.2$. In the latter case, the lowest eigenvalue is no longer a separated point, but rather can be ascribed to the band. At $J=0.3$ it becomes quite clear that the lowest eigenvalue belongs to the continuum spectrum. Finally, the picture at $J=1$ is almost a picture for free fermions with the Fermi momentum $p_F=\pi/2$ and with the lowest branch $E_{\min}(P)$ close to $J|\cos(P)|$.

The proposed mechanism of the transition implies that critical value of J is determined by the energy Δ of the lowest defect at $J=0$. Our 2D results are summarized in the Table I. It shows for comparison the middle point J_m of the critical interval δJ and the zero- J gap Δ for all cases we have studied. One can see that both J_m and Δ change by a factor of 10 depending on the filling factor and the type of the interaction potential.

However, their ratio J_m/Δ is almost constant and is close to 0.5 in all cases. Since we assume that $J_m\rightarrow J_c$ with increasing cluster size, this implies an empirical rule for J_c :

$$J_c = \beta \Delta_\infty, \quad (4)$$

where β is some number that is close to 0.5, and Δ_∞ is the smallest energy necessary to create a point defect in an infinitely large system.

C. Study of the size effect

1. Classical size effect

As can be expected from Table I, the energy Δ of the lowest excited state at $J=0$ may have much influence on J_m . We show here that Δ may have a strong size dependence in small clusters. This kind of a size effect can be called “classical.”

The SR and LR potentials are very different in this aspect. In the case of SR interaction the defect with the lowest energy is the point defect [see Fig. 1(b)]. The weak dependence of Δ on the cluster size is only due to the interaction of the defect with its images, which appear as a result of the periodic boundary conditions.

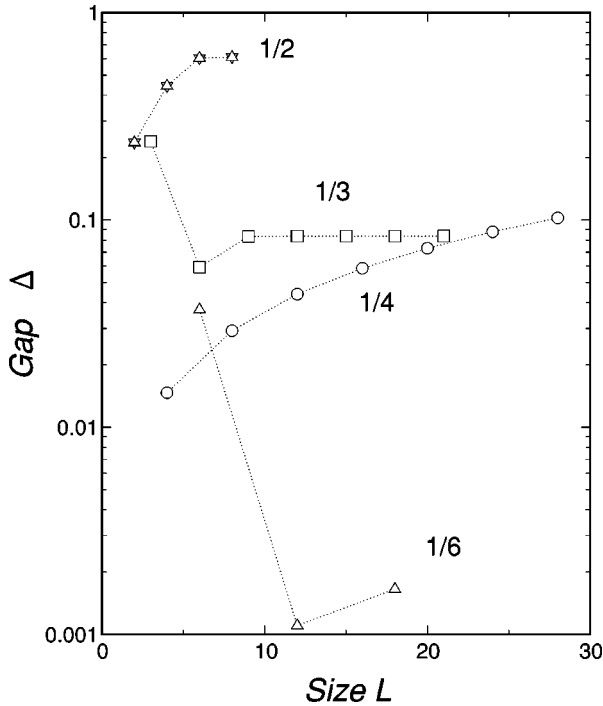


FIG. 8. Size dependence of the lowest excitation energy at $J = 0$ for different filling factors as obtained by classical Monte Carlo simulation. The saturation occurs at such size when the point defect becomes the lowest excitation.

In the case of LR interaction the energy Δ depends strongly on the size of the cluster for relatively small clusters. This dependence becomes stronger for smaller filling factors. One can see in Fig. 1(a) that in the 4×6 cluster at $\nu = 1/2$ the point defect appears only as the fifth icon. At $\nu = 1/6$ the five lowest-energy icons shown in Fig. 1(c) do not contain a point defect at all.

We have studied thoroughly the low-energy spectrum for LR interaction at $J = 0$. The square clusters with different sizes L and filling factors $1/2$, $1/3$, $1/4$, and $1/6$ were analyzed using classical Monte Carlo technique. The results are presented in Fig. 8. At $\nu = 1/3$ and $1/6$ new low-energy types of dislocations appear with increasing the cluster size. These dislocations are restricted by the periodic conditions in smaller clusters. As a result, Δ decreases with size for small clusters. However, for large enough clusters new dislocations cease to appear, so that Δ does not decrease. Since the energy of a dislocation is proportional to the size of the cluster, the point defect should win the competition in large enough clusters.

For $\nu = 1/2$ and $1/3$ the point defect becomes the lowest excited state starting with the sizes 6×6 and 9×9 , respectively. For $\nu = 1/4$ and $1/6$ we are unable to find this critical size. However, the increase of Δ with L ensures that the point defect should eventually become the lowest excited state.

Our conclusion is that in the case of LR interaction one should expect a significant size effect in J_m due to the classical size effect in Δ .

2. Quantum size effect

Since the classical size effect is negligible for the SR interaction we can analyze the ‘‘quantum’’ contribution to

the size effect in J_m comparing the results for different clusters. The size dependence of J_m for the SR potential can be estimated from Fig. 3(b).

We study only the clusters with the dimensions commensurate with the primitive vectors of the WC. Otherwise the periodic continuation destroys the crystalline order. For $\nu = 1/2$ this requires that both L_x and L_y are even. Since we can study clusters up to 16 particles this condition restricts our options to 4×4 , 4×6 , and 4×8 clusters.

The low-energy spectrum for the 4×4 cluster is shown in Fig. 5. In this case the WC icon generates quasimomenta $\mathbf{P} = (0, 0)$ and (π, π) . The flux sensitivity and the ground-state splitting are shown in Fig. 3(b) for all three clusters studied. One can see that the data do not show any pronounced systematic size dependence of J_m , suggesting that for the SR potential J_c is within the interval $0.015 - 0.025$.

Thus, we have found that the size effect at a given value of Δ is small. Assuming this result to be independent of the type of potential, one can suggest that for the LR interaction the ‘‘classical’’ contribution to the size effect is the major one. Then one can use Eq. (4) to estimate J_c for the LR potential using the classical energy Δ_∞ . For $\nu = 1/2$, say, we get $\Delta_\infty = 0.61$ (see Fig. 8) resulting in $J_c \approx 0.3$. To get a reliable estimate for this case from the quantum computations one should consider at least a 6×6 cluster since the point defect becomes the lowest excited state starting with this cluster size.

D. Gap at nonzero J

Now we analyze the gap between the split ground state and the excited states that belong to the defect band. This gap is clearly seen in Figs. 2(a), 2(b), 4(a), and 5. At large J the branches have a form of beams with different slopes. These slopes definitely come from the confinement quantization of free fermions.

The large number of states in each beam reflects high degeneracy of the free-fermion ground state at $\nu = 1/2$. For example, in Fig. 5 all lines that are horizontal at large J are the states that are degenerate for the free fermions. The splitting of these states is a result of interaction. The gap between the split ground state and the bunch of the states in the same beam can be easily calculated in the mesoscopic region of large J , where $4\pi^2 J/L^2 \gg 1/L$. The picture of beams is valid in the same region and it does not imply the existence of a gap at large J in a macroscopic system.

On the other hand, the gap Δ at $J = 0$ is the energy of defect and it has a nonzero limit in a macroscopic system. Thus, an important question arises, whether or not the gap has a nonzero limit right after the IM transition. The nonzero gap would mean that the state after the transition is superconducting.

We have put a lot of computational effort into answering this question but the results are still inconclusive. Our best achievement is shown in Fig. 5 where we compare the results for 4×4 and 4×8 clusters. The confinement quantization would prescribe that the gap decreases in half. We have found that the gap for the 4×8 cluster is less than for the 4×4 cluster but the ratio is significantly larger than 0.5.

IV. CONCLUSIONS

We have performed a numerical study of the structural and IM phase transitions in 2D fermionic systems with Hamiltonian Eq. (1). The structural transition has been detected by studying the splitting of the ground state, degenerate in the crystalline phase. Simultaneously we studied the IM transition by computing the sensitivity of the ground-state energy to the boundary conditions. In the 2D case we have studied the systems with LR and SR interactions at different filling factors. Within the accuracy determined by the size effect the IM transition occurs simultaneously with the structural transition.

We argue that the structural transition on a lattice is not of the first order in all cases considered. We think that the origin of the transition is an avoided crossing of the ground state and the defect states in the Wigner crystal with the same total quasimomentum. This simple picture implies that

the critical value of J is determined by the defect with the lowest energy Δ at $J=0$. To illustrate our point the data for the 1D system with Coulomb interaction are also presented. The possibility of the delocalized phase above the transition to be superconducting is discussed.

We have found that the size effect is not very strong for J_c in the case of the SR interaction. For the LR interaction it is strong because of the size dependence of the defect energy Δ . We argue that a reliable estimate for J_c from finite-cluster computations in this case can be obtained with the use of the empirical rule Eq. (4).

ACKNOWLEDGMENTS

We are grateful to A. P. Levanyuk and E. I. Rashba for helpful discussions. We acknowledge the support of UCSB, Subcontract KK3017 of QUEST, and the support of the San Diego supercomputer center.

-
- ¹A. L. Efros, F. G. Pikus, *Solid State Commun.* **96**, 183 (1995).
²R. Berkovits and Y. Avishai, *Europhys. Lett.* **29**, 475 (1995).
³D. L. Shepelyansky, *Phys. Rev. Lett.* **73**, 2607 (1994); Y. Imry, *Europhys. Lett.* **30**, 405 (1995).
⁴X. Zhu and S. G. Louie, *Phys. Rev. B* **52**, 5863 (1995), and early references quoted therein.
⁵E. Dagotto, *Rev. Mod. Phys.* **66**, 763 (1994).
⁶R. T. Scalettar, G. G. Batrouni, A. P. Kampf, G. T. Zimanyi, *Phys. Rev. B* **51**, 8467 (1995).
⁷A. van Otterlo, K.-H. Wagenblast, R. Baltin, C. Bruder, R. Fazio, and G. Schon, *Phys. Rev. B* **52**, 16 176 (1995).
⁸E. Roddick and D. Stroud, *Phys. Rev. B* **51**, 8672 (1995).
⁹E. S. Sorensen, E. Roddick, *Phys. Rev. B* **53**, 8867 (1996).
¹⁰M. Girardeau, *J. Math. Phys.* **1**, 516 (1960).
¹¹C. N. Yang and C. P. Yang, *Phys. Rev.* **147**, 303 (1966); **150**, 327 (1966); **151**, 258 (1966), and earlier references quoted therein.
¹²J. des Cloizeaux, *J. Math. Phys.* **7**, 2136 (1966).
¹³B. Sutherland and B. S. Shastry, *Phys. Rev. Lett.* **65**, 1833 (1990).
¹⁴F. G. Pikus and A. L. Efros, *Solid State Commun.* **92**, 485 (1994).
¹⁵W. Kohn, *Phys. Rev.* **133**, A171 (1964).
¹⁶D. J. Scalapino, S. R. White, S. Zhang, *Phys. Rev. B* **47**, 7995 (1993).
¹⁷E. V. Tsiper and A. L. Efros, *J. Phys.: Condens. Matter* **10**, 1053 (1998).
¹⁸L. D. Landau and E. M. Lifshitz, *Statistical Physics*, Part 1 (Pergamon Press, 1980), 3rd. ed., p. 459.
¹⁹E. V. Tsiper, F. G. Pikus, and A. L. Efros, (unpublished); *cond-mat/9512150*. (1997).
²⁰A. F. Andreev and I. M. Lifshitz, *Zh. Eksp. Teor. Fiz.* **56**, 2057 (1969) [*Sov. Phys. JETP* **29**, 1107 (1969)].
²¹E. V. Tsiper and A. L. Efros, *J. Phys.: Condens. Matter* **9**, L561 (1997).
²²D. Poilblanc, S. Yunoki, S. Maekawa, and E. Dagotto, *Phys. Rev. B* **56**, R1645 (1997).